

Clay and Magnetic Sand Biomass Based Composite for Methylene Blue Adsorption (Effects of Composition Ratios of Functional Materials and Synthesis Conditions)

Mih Venasius Nsom, Ekane Peter Etape^{*}, Beckley Victorine Namondo, Josepha Foba-Tendo, Lena Yoh Elango Ekaney

Department of Chemistry, Faculty of Science, University of Buea, Buea, Cameroon

Email address:

ekane20022001@yahoo.fr (E. P. Etape)

^{*}Corresponding author

To cite this article:

Mih Venasius Nsom, Ekane Peter Etape, Beckley Victorine Namondo, Josepha Foba-Tendo, Lena Yoh Elango Ekaney. Clay and Magnetic Sand Biomass Based Composite for Methylene Blue Adsorption (Effects of Composition Ratios of Functional Materials and Synthesis Conditions). *American Journal of Nanosciences*. Vol. 7, No. 4, 2021, pp. 82-95. doi: 10.11648/j.ajn.20210704.13

Received: October 28, 2021; **Accepted:** November 17, 2021; **Published:** November 25, 2021

Abstract: In recent times, iron oxide based magnetic nanoparticles (mainly magnetite (Fe_3O_4) or maghemite ($\gamma\text{-Fe}_2\text{O}_3$)) as well as clay and clay based composites, have become very important in the elimination of persistent organic compounds from waste water systems. This has been carried out by magnetic assisted chemical separation (MACS) process. The feasibility of using two locally sourced materials: magnetic black sand from down beach Limbe and clay from Bamessing Ndop for the removal of methylene blue (MB) dye from aqueous solution have been studied. The effects of contact time, pH, adsorbent dosage, temperature, grinding / length of grinding, composition ratios of the functional materials such as peel, pectin and starch, hydrothermal carbonization and concentration of dye solution were investigated. The test samples have exhibited great potentials for use in waste water purification for the removal of persistent organic compounds such as methylene blue dye. The results revealed that, varying various compositional ratios of the functional materials such as peel, pectin and starch to increase their affinity, selectivity, or degradation capacity towards targeted compounds influenced the activities of the adsorbents. The results also indicated that maximum performance was reached at pH value of 8 for Iron oxide (sand) based adsorbents and 12 for clay based adsorbents. Grinding / increase in grinding time have shown positive effects on the adsorbent properties of the composite from black sand and maximum grinding time varied depending on the compositional ratios of functional materials. Also within a certain threshold, hydrothermal carbonization improved on the adsorbent efficiency of the samples formulated with saccharides. The adsorption kinetic of methylene blue onto the adsorbents could be better fitted by the linear Langmuir isotherm and the pseudo-second-order model was a better model fitting the kinetics of the adsorption in this study.

Keywords: Methylene Blue, Magnetic Sand, Iron Oxide, Clay, Hydrothermal Carbonization

1. Introduction

Water is a prime need of life but clean water for house hold use has continuously decreased especially around industrial city centers. Coloured Industrial effluents such as dyes constitute the major pollutants of waste water from the textile industries. The use of cationic dyes in technology and innovative science is not to be over emphasized. Cationic dyes with high water solubility have been given many diverse applications such as the dyeing of paper, cotton, wool, and hair. The discharged of synthetic dyes in industrial

effluent has far reaching polluting effects on the aquatic environments in particular and the ecosystems in general. Exposure to lethal doses of cationic dyes such as methylene blue may lead to vomiting, cyanosis, jaundice, shock, and tissue necrosis in humans [1]. A way of solving the problem is by treating the waste water. Unfortunately, most classical waste management methods for adsorption of dyes used in industries have failed due to their stability to light and oxidizing agents, and resistance to aerobic digestion [2, 3]. Amongst several methods such as the electrochemical, coagulation, flocculation, chemical oxidation, solvent

extraction, and adsorption [4–6], the adsorption method has singled out itself for contaminant removal due to its operational simplicity and cost-effectiveness. The available commercial adsorbents such as zeolites and activated carbon have proven to be effective but expensive and have problems of regeneration capacity. Physicochemical properties of adsorbent and regeneration capability have been known to limit the efficiency of adsorption processes. These difficulties have opened doors for continued interest in the development of biomaterial adsorbents derived from renewable sources such as cellulose, pectin, starch, chitosan and their composites with metal oxides.

Textile printing and dyeing industries such as Cotonniere Industrielle du Cameroun (CICAM) in Douala, Cameroon, and other industries in the same family in other parts of the world are water-intensive and require large volumes of freshwater at various steps of printing which lead to the release of large volume of wastewater. The quest for cheap, available and eco-friendly agro-based biopolymers adsorbents has led to the interest in biomaterials such as pectin, chitosan and alginates which have all shown good adsorption capacities [7, 8] attributed to hydroxyl and carboxylate groups. However, a common drawback to the use of these biopolymers is their biodegradability without adequate strength and physical stability required for good adsorption.

In keeping with the fact that they can be extracted in large volumes from agricultural waste using low-cost methods, an approach to improve the mechanical, chemical, and physical performance of biopolymers has been adopted. This method incorporates them on the surfaces of other adsorbent materials especially Nano sized magnetic metal oxide particles such as iron oxide which offer the possibility of using magnetic fields to facilitate the separation of adsorbent from treated waters [9]. The coast of the Atlantic Ocean such as the sandy beach of Limbe Cameroon, holds large deposits of magnetic fractions of black sand. The Magnetic fractions of black sand are rich in iron-oxide nanoparticles which are potential adsorbent materials. However, iron-oxide is easily oxidised and difficult to handle. This problem can be solved by coating the particles with more stable polymer sheaths using substances such as pectin and starch. Simultaneously, like Iron Oxide based sorbents, clay sorbents are becoming popular for wastewater treatment [10, 11]. Clay minerals are abundant in availability, low in cost, and classified as an environment friendly material. These properties coupled with their distinct physical and chemical characteristics, have transformed them into the ultimate choice for the sorption process. Therefore, clay can substitute low-performance bio sorbents as well as costly activated carbon [12]. Clay sorbents may be used as such or in modified form depending upon the nature of the target pollutants [13, 14]. Due to its geographical location, Bamessing Ndop in Cameroon possesses a great variety of clay minerals but sorption potential of these clays, especially brown clay (BC), has not been investigated. Removal of organic pollutants from aqueous environments is primarily

controlled by hydrophobic interactions at the interfaces of the sorbate and sorbent depending upon the carbon content of the sorbent rather than the mineral part of the clay sorbents [15, 16]. This is suggesting that modification of clay by biopolymer coating can significantly improve its surface properties, thereby improving its water-decontaminating efficiency. Biopolymers are particularly interesting because of their biocompatibility, biodegradability, and nontoxicity. Combining the adsorption properties of some biomaterials such as pectin, starch, and magnetic properties of iron oxide seems very interesting. Therefore the present study was intended to evaluate the activity of both Iron Oxide based composites from black sand and brown clay based sorbents, to investigate optimal values of various factors such as sorbent dose, pH, contact time, initial dye concentration, hydrothermal carbonization and temperature required for maximum removal of MB dye from aqueous environments. Furthermore, we have studied the sorption kinetic equilibrium, to understand equilibrium properties and the mechanism of the sorption process.

2. Experimental

2.1. Materials

The waste was obtained from the discharge process of a chemical enterprise in Douala, black sand from down beach Limbe, Cameroon, Clay from Bamessing Ndop, Cameroon. Sulfuric acid (H_2SO_4 , 96%), Pectin (d-galacturonic acid) from Sigma-Aldrich, starch (native) from the Douala market and lemon peels.

2.2. Experimental Methods

2.2.1. Sample Collection and Preparation

The location sampling sites at the sandy beach of Limbe and the Bamessing clay deposit are shown on Figure 1.

Sand from Limbe sandy beach:

The sand was collected from the Limbe sandy Beach located in Fako Division, South West Region of Cameroon. The sand collected from the beach was air dried for 3 days to reduce the wetness and oven dried at 60°C for 4 hours. The oven dried sand was cooled to 25°C and subjected to magnetic separation to isolate the magnetic fraction.

b) Clay collection and preparation

Clay samples were collected from Bamessing and Bamunka Situated in the Ndop plain (with depth ranging from 3 to 4 m). Representative Drills are coded N– in Figure: 2. On the drill core profiles, important clayey materials with different faces show colour and textural variation. The Colour changes observed were brown, grey, dark grey, mottled to yellowish brown, and the texture from clayey to sandy. Dark Grey clays were mostly found at the foot of hills in Bamessing, and brown clays around Bamunka. Sampling of clays was based on the following parameters: the thickness of the clayey layer, colour and grain size and Six representative samples were collected for analyses.

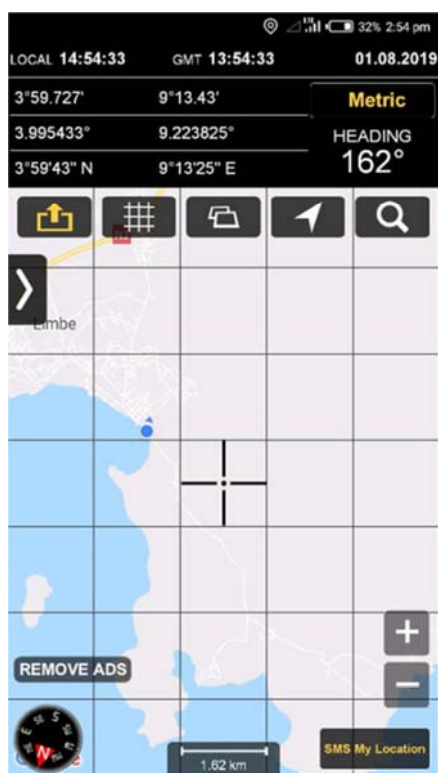


Figure 1. Limbe sandy beach Showing specific collecting points.

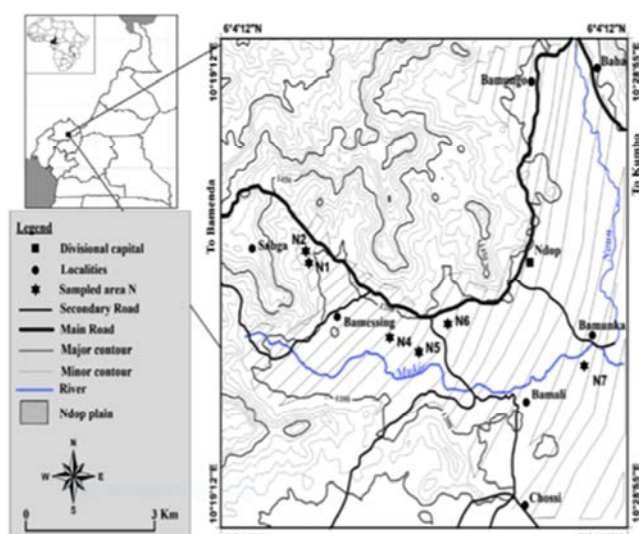


Figure 2. Drills location map of the study area, Bamessing NDOP sampling positions.

2.2.2. Lemon Peels Collection and Extraction of Pectin

The lemon was bought from the farm, washed under running tap water and dried. The lemon was peeled using a kitchen knife and Pectin was extracted from lemon peels. The extraction was done with the help of distilled water, hydrochloric acid and cheese cloth.

2.2.3. Synthesis of Starch-pectin or Peels Magnetite Nano Hybrid Composites

The Synthesis of starch-pectin or peels magnetite Nano hybrid composites was as previously discussed [17] but with modifications. A 10% (w/v) pectin solution was prepared by dissolving 6g of pectin powder into hot distilled water at 60°C while stirring to ensure complete dissolution. The volume of the solution was made up to 60ml while from the 10% pectin solution, 9ml was measured into a 500ml volumetric flask and made up to the mark with distilled water to give a concentration of 0.18% pectin solution. Also a 0.86% pectin solution was prepared by measuring 17.2ml of the 10% pectin solution into a volumetric flask and diluting with distilled water to 200ml. A 10% (w/v) starch solution was prepared by dissolving 10g of powder starch in 100ml of hot distilled water at 60°C while stirring to ensure homogeneity. A 0.18% starch solution was prepared by diluting with distilled water, 13.5ml of the 10% (w/v) starch solution into a 750ml capacity flask, while a 0.86% starch solution was prepared by diluting with distilled water, 51.6ml of the 10% (w/v) Starch solution into another 750mL flask. The synthesis of the magnetic fractions of sand (Fe_3O_4)-starch-pectin Nanohybrid composites was carried out at room temperature without purging as is usually the case with the synthesis of iron oxide nanocomposites. Methylene blue was chosen as a model dye due to its well-known characteristics such as its relative stability compared with other dyes and strong adsorption onto solids. The use of ammonia solution was for amidation of the pectin and to cause de-esterification reaction at the polymer esterified group during the co-precipitation of iron ions. This was to provide more binding sites for magnetite nanocomposites. The synthesis of Fe_3O_4 using the co-precipitation method in the presence of starch/pectin or starch/ peels mixture is expected to initiate the covalent linkage instantaneously. This in effect should prevent further particle growth, resulting in starch/pectin-coated ferrite composites with a closer control over particle size. The magnetic fraction of the sand was mixed with the extracted pectin and starch and milled for 15 minutes per sample to form a composite. The sample code and formulation (components were mixed in the ratios) are shown on Table 1.

Table 1. Sample formulation (components and ratios in which they were mixed).

Sample code	Oxide-polymer Ratio Oxide: Polymer	Oxide (g)	Starch (g)	Pectin (g)	% by mass of oxide	%by mass of polymer	% by volume of oxide	% by volume of polymer
UBM21A	4: 1	20.0	0.50	0.50	95.24	4.76	80.00	20.00
UBM22B	1: 1	15.0	3.00	/	83.33	16.67	50.00	50.00
UBM23C	1: 1	15.0	/	3.00	83.33	16.67	50.00	50.00
UBM24D	1: 1	15.0	1.50	1.50	83.33	16.67	50.00	50.00
UBM25E	1: 1	15.0	2.25	0.75	83.33	16.67	50.00	50.00
UBM26F	1: 4	1.0	7.00	7.00	6.67	93.33	1.44	98.56

Approximate density of polymer=1g/cm³, Approximate density of oxide=5g/cm³

2.2.4. Hydrothermal Carbonization

In each experimental run, about 5 g of Composite/starch: pectin was introduced into a non-stirred 40 ml stainless steel Teflon-lined reactor with an external heater. The process conditions (dosage of additive, reaction temperature and reaction time) are summarized in Table 2. The reactor was heated to 180°C or 200°C with a heating rate of 10°C/min. The temperature was maintained under an autogenic pressure for a period of 2 hours. The raw product was obtained by

cooling the reactor to room temperature. The raw product was washed with 150 mL of distilled water, filtered by filter paper and the hydrochar/Iron Oxide composite dried at 105°C for 3 h. The hydrochar (Hc) characterized by Fourier-transform infrared spectrometer, elemental analyzer and thermogravimetric analysis was used without pretreatment. The yield of hydrochar was calculated using equations (1).

$$(Hc \%) = \frac{\text{Hydrochar weight}}{\text{Weight of Iron oxide, starch:pectin composite}} \quad (1)$$

Table 2. Process conditions (dosage of additive, reaction temperature and reaction time) for hydrothermal carbonizations.

Code	Ratio Oxide: polymer	Hydrothermal Carbonization (HTC)			
		Temperature (°C)	Initial mass (g)	Reaction time (hrs.)	Sulphuric acid (ml)
UBM21A	4: 1	160	5.000	2	0.0
UBM21A	4: 1	175	2.000	2	3.0
UBM21A	4: 1	190	1.100	2	3.0
UBM24D	1: 1	160	3.000	2	3.0
UBM24D	1: 1	175	0.900	2	3.0
UBM24D	1: 1	190	1.100	2	3.0

2.2.5. Adsorption Measurements of Methylene Blue

0.5 g of ground dried hybrid composites were put in 100 mL of methylene blue solution of 25 mg/L. This mixture was maintained at room temperature and continuously shaken at about 300 rpm for 2 hours with the help of a Burrell Wrist Action Shaker. After 2 hours, the methylene blue uptake onto the hybrid composite was calculated from the difference between the methylene blue concentration before and after adsorption onto the hybrid composite.

2.2.6. Characterization Techniques

FTIR spectra were recorded in the middle infrared (4500cm⁻¹ to 500cm⁻¹) on Shimadzu Prestige 21 with a resolution of 4cm⁻¹ in the absorbance mode for 8 to 128 scans at room temperature. The ASCI data were plotted using OriginLab 7.0 software while the TGA were carried out using a Pyris 6 PerkinElmer TGA 4000-Thermal Analyzer under nitrogen atmosphere with a flow rate of 20mL/min and temperature range of 10°C to 900°C at an increase rate of 10°C/min. The determination of the microstructure was carried out by powder X-ray diffraction measurements (PXRD). The PXRD patterns of composite were recorded on a Philips PWO₄ Xpert pro X-ray diffractometer. The

X-ray source was Cu-Kα with a voltage of 40kV and a current of 30mA. The measurement was in the scanning range of 0–80 at a scanning speed of 50s⁻¹. The concentrations of methylene blue solutions were analyzed by measuring their absorbance at 662nm on a Perkin-Elmer UV/Vis spectrophotometer. This wavelength corresponds to the maximum absorption peak of the methylene blue monomer.

3. Results and Discussions

3.1. PXRD and EDS/XRF of the Black Sand from Down Beach Limbe

EDS/XRF

The EDS/XRF of the black sand from the sandy beach of Limbe is presented in Figure 3. The results revealed that TiO₂ and Fe₂O₃ were the two minerals in significant quantities and which were of particular interest because the catalytic properties of TiO₂ as well as the magnetic properties of Fe₂O₃ could be exploited separately in the purification of waste water. However, our work seeks to exploit only the magnetic properties of the Fe₂O₃.

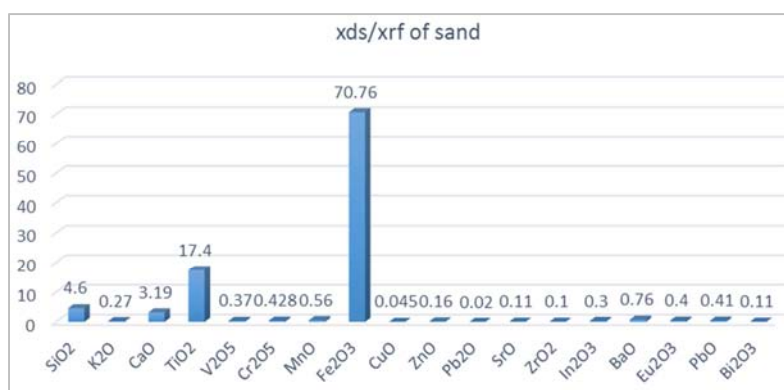
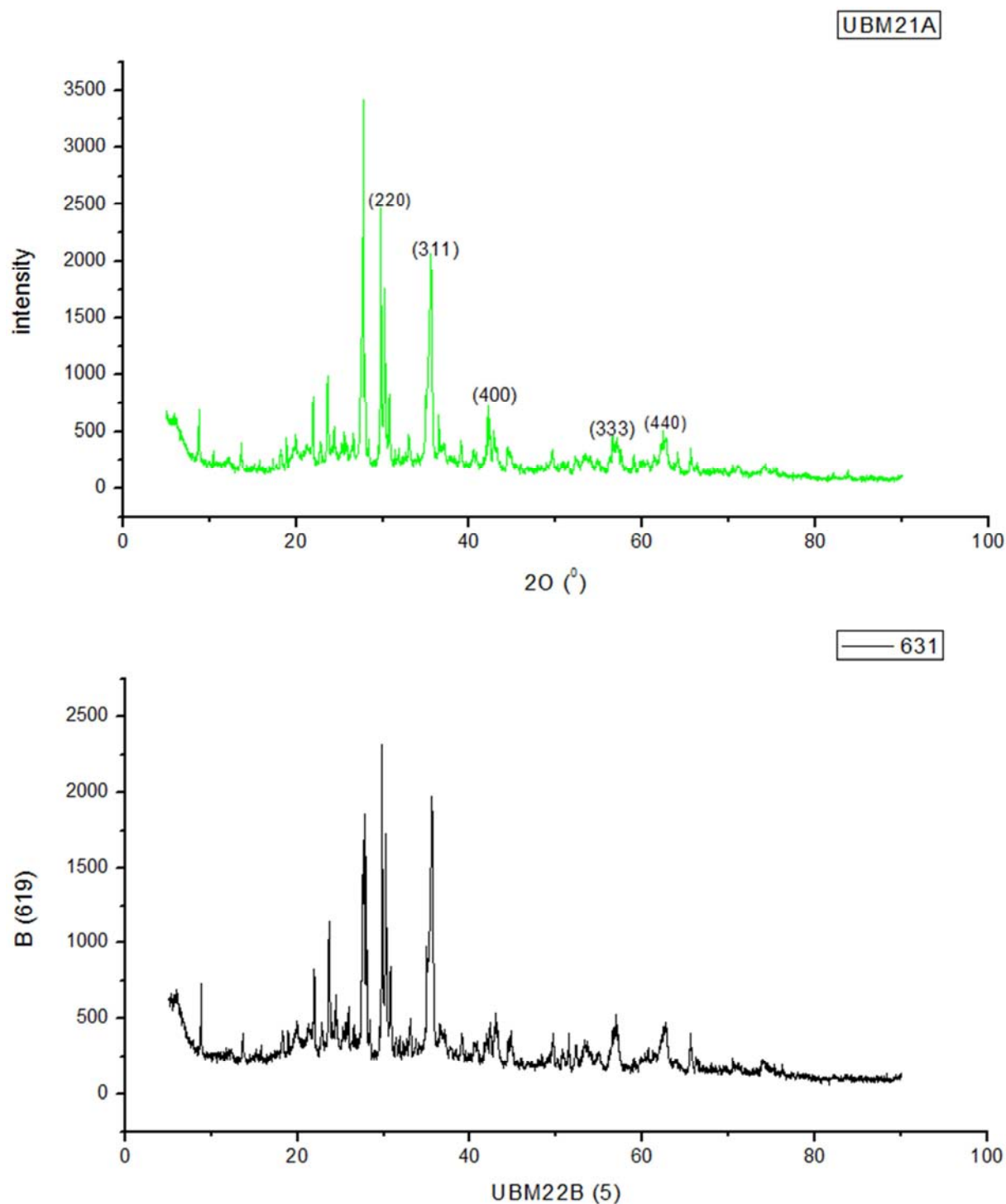


Figure 3. EDS/XRF showing the fractions of metal oxides in the sampled sand.

XRD of the treated sand samples

The sample codes as per compositions are shown on Table 2 while the PXRD patterns of the synthesized samples with Variation in Composites of Oxide/ Polymer ratio, Pectin: starch ratio, polymer and NMP oxide concentration by mass (Hybrid Composites) are shown in Figure 4. The samples MV20A, MV21B, MV23C, MV24D and MV25E, have diffraction peak at $2\theta=30.2^\circ$, 35.5° , 43.1° , 57.0° and 62.4° assigned to (220), (311), (400), (511) and (440) lattice planes

of the cubic structure. The diffractions at angle $2\theta=35.5^\circ$ could be assigned to Fe_3O_4 , face centered cubic structure which matched with JCPDS card no. 85 1436 and indicating that the isolated samples from the black sand were Fe_3O_4 , face centered cubic structure. These results also suggested that, there was the formation of an inverse spinel Fe_3O_4 , based structure with a pure magnetite phase which persisted even in the presence of saccharide particles.



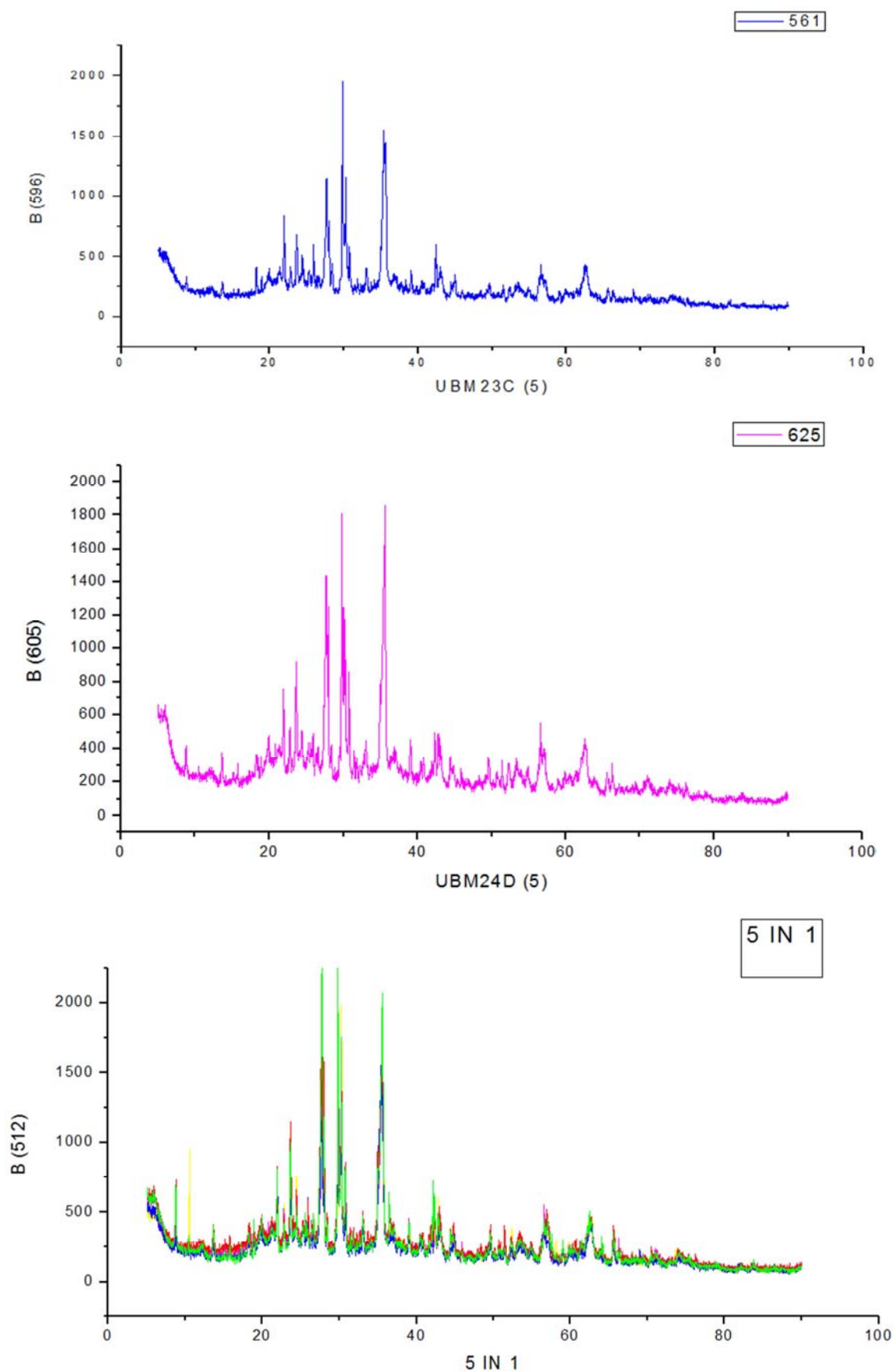


Figure 4. Variation in: Composites of Oxide/ Polymer ratio, Pectin: starch ratio, polymer and NMP oxide concentration by mass (Hybrid Composites).

The determination of crystallites sizes was done using Debye-Scherrer's equation (equation (2)) which measured the size of particles according to broadening of the most intense peak (311) in PXRD profile shown in Figure 3.

$$D = \frac{k\lambda}{\beta \cos \theta} \quad (2)$$

Where k is a dimensionless shape factor, λ is the x-ray wavelength, β is the line broadening at half the maximum intensity (FWHM) and θ is the Bragg angle.

Particle sizes of the samples (MV21A, MV22B, MV23C, MV24D and MV25E) were determined as 10.2nm, 9.7nm, 10.3nm, 9.6nm and 9.6nm respectively. The results suggested that the synthesized samples were all Nano particles.

3.2. Fourier Transformed Infrared (FT-IR) Spectra Characterization

The FT-IR profiles of MV22BB (Hybrid composites before adsorption) and MV22BA (hybrid composites after adsorption), PEC001 and STA001 are shown in (Figure 5). The spectra of PEC001 and STA001, represent the profiles of pectin and starch samples respectively and showed all familiar peaks while the Hybrid composites MV22BB, shows the Fe – O bond vibration of Fe_3O_4 from the sand and the symmetric / asymmetric carboxylate – metal (COO-Fe) linkage [19]. The chemical activity on the surface of the adsorbents on the surface of samples MV22EB and MV22EA was demonstrated by similar peaks with small shifting indicating the presence of methylene blue adsorption on the

surface of the adsorbent. The FTIR spectra of the Iron oxide hydrochar presented on Figure 6 shows a band at 3438 cm^{-1} which was attributed to -OH stretching vibration in hydroxyl groups while Asymmetric and symmetric -C-H stretching of methylene groups were identified at 2922 cm^{-1} and 2864 cm^{-1} respectively. The band at 1698 cm^{-1} implied the stretching vibration of -C=O in ketone and amide groups [19] while the peak at 1450 cm^{-1} was assigned to the -C=O stretching in aromatic ring carbons. In addition, the peak at 910 cm^{-1} was attributed to the out-of-plane bending vibration in aromatic nucleus -CH structure, which suggested the occurrence of aromatization during HTC process [19]. The other peaks at 1159 cm^{-1} and 1123 cm^{-1} were attributed to symmetric and asymmetric stretching of sulfonated groups, respectively. S-O stretching at 1370 cm^{-1} , asymmetric C-S stretching at 910 cm^{-1} and S-O bending vibration at 660 cm^{-1} are related to sulfonic acid group [20] resulting from the introduction of sulfonic acid group in the HTC process. The FTIR for the hydrochar are indicating the formation of a more stabilized composite with aromatization. The hydro chars for MV21A-MV25E hybrid composites after adsorption indicated broadening of the band with peak at 3299 cm^{-1} . This change could be attributed to the newly established intermolecular hydrogen bonding between neighboring hydrochar and newly introduced methylene blue molecules. The level of broadening varies with the pectin: starch ratio as well as the polymer concentration in the hydrochar composite which was to be expected since the hydrochar is a product of the heat treatment of Saccharides.

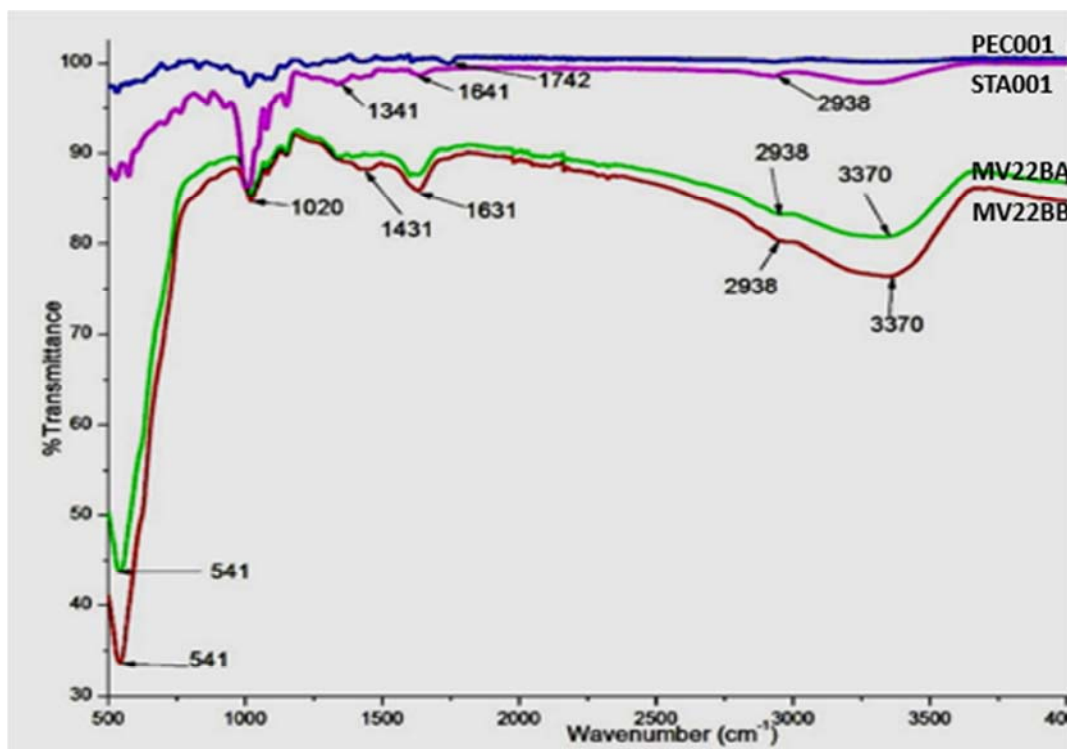


Figure 5. FT-IR Spectrum of MV002_NP (Composites with starch pectin/ ratio of 1: 4 at polymer concentration of 0.18%) Hybrid composites before adsorption (MN002_NP) and after (MV010_NP) Adsorption.

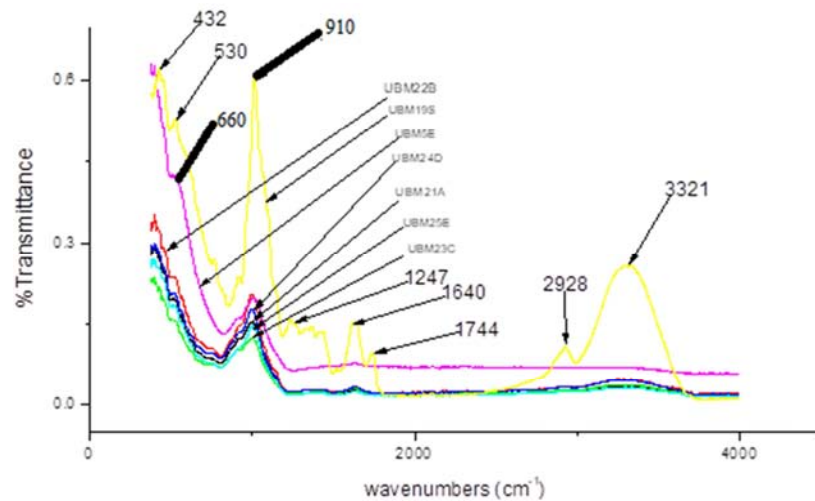


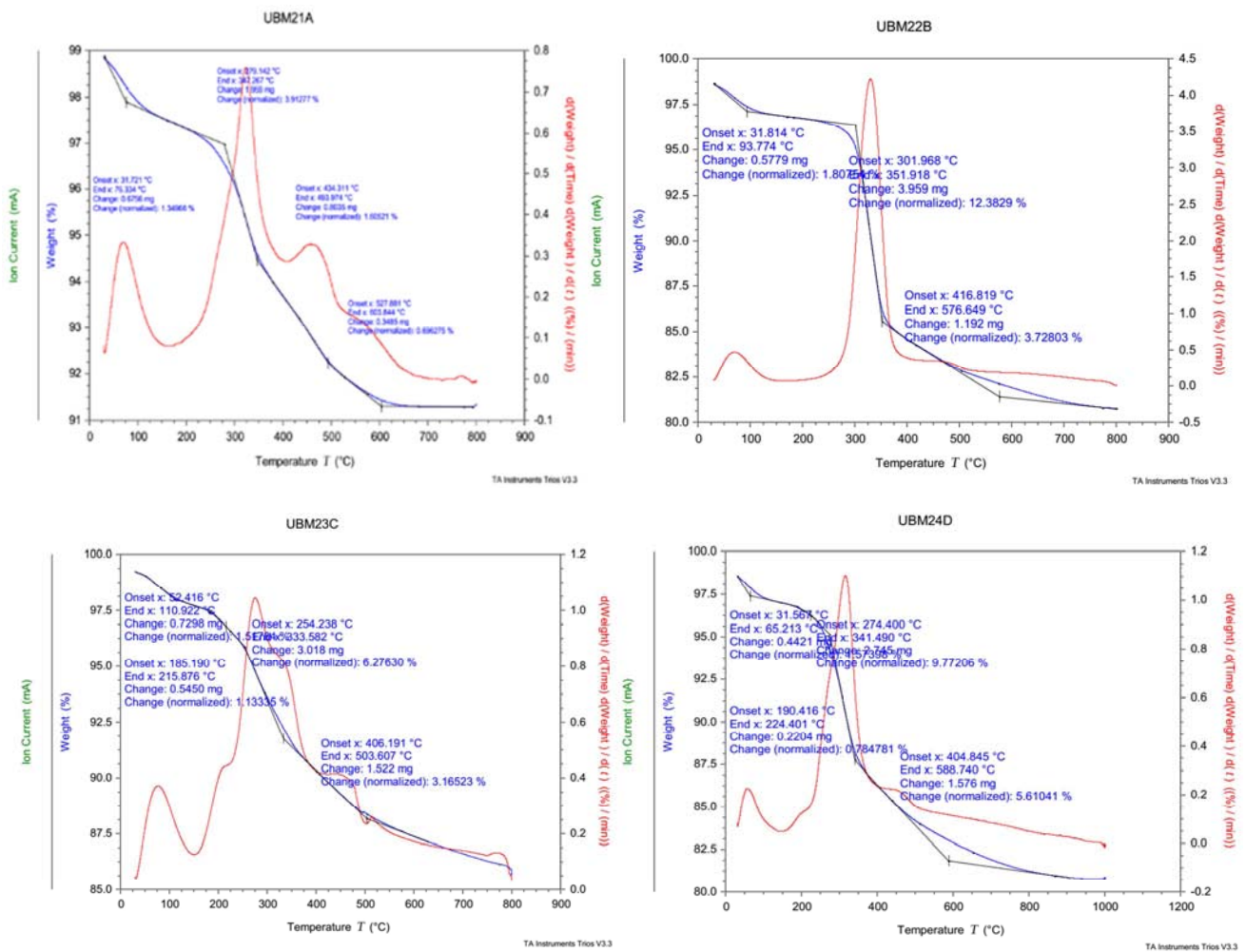
Figure 6. FTIR of hydrothermally carbonized Iron oxide composite.

3.3. Heat Treatment

Hydrothermal Characterization (HTC)

Figure 7 illustrates the combustion profiles of the hydrochar and for a better evaluation of the different combustion behaviors, the entire combustion profile was

divided into four stages according to the rate of weight loss in the DTG curve while Table 3 lists the combustion stages, characteristic temperatures and residue of the Iron Oxide/hydrochar.



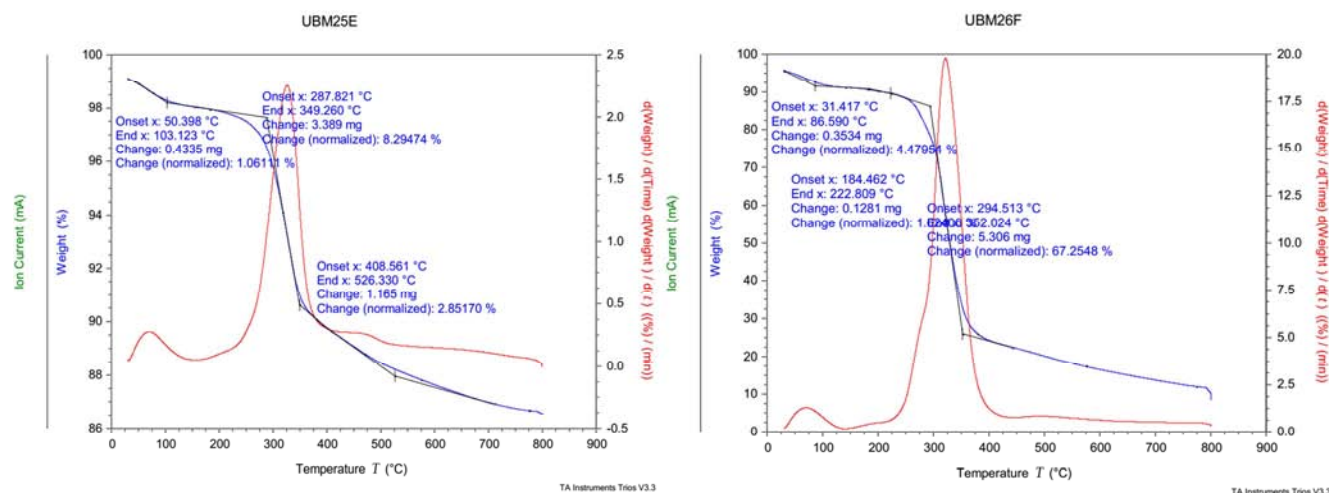


Figure 7. TG-DTG curves for combustion profiles of the hydrothermally carbonized composite. Notes, temperature range, 20°C - 800°C; heating rate, 20°C/min; air flow rate, 20 mL/min; an atmospheric pressure.

Table 3. Combustion stages, characteristic temperatures and residue of the hydrochar.

	Stage 1 (°C)	Stage 2 (°C)	Stage 3 (°C)	Characterization temperature			Residue (wt. %)
				T _i (°C)	T _m (°C)	T _b (°C)	
Iron Oxide /Hydrochar	85	85-340	340-645	187	385	657	45-70

Notes, Stage 1—Dehydration process, Stage 2—Devolatilization and combustion phase, Stage 3—Char combustion phase, Last stage—Burnout phase, T_i—Ignition temperature, T_m—Maximum combustion rate temperature, T_b—Burn out temperature (T_b).

The decomposition profile of the hydrochar was observed in the temperatures range 85°C - 657°C. The first peak at 85°C was attributed to moisture content while that in Stage 2 in the temperature range of 85°C - 340°C was attributed to devolatilization and combustion. The third stage occurred in the temperature interval of 340°C - 645°C generated the final product (the char). The Fuel ignition temperature (T_i) is a critical parameter to minimize fire and explosion [21]. The Fuel ignition temperature of the hydrochar was 185°C while the DTG peak temperature was 384°C. The temperature at which the rate of weight loss diminished to 1% wt. /min at the end of the combustion profile was 657°C, suggesting that it had a high heating value. These observations are derived from the fact that the hydrochar is a consequence of hydrothermal carbonization of saccharides which was accompanied by dehydration, condensation, or polymerization and aromatization reactions. This results indicated that the char needed a long reaction time to achieve the maximum decomposition rate and so has a stabilizing effect on the initial composite material. As a consequence, modifying the synthesis conditions (i.e., the concentration of the aqueous saccharide solution (S: P ratio), the temperature of the hydrothermal treatment, the reaction time, and type of saccharide) have a direct influence on the performance of the hydrochar as an adsorbent.

The TGA profiles of the hybrid pectin-starch magnetite (not hydrothermally carbonized) showed similar results to the hydrothermally carbonized samples but with a little decrease in the temperatures of the decomposition of the various

intermediates. This was an indication that hydrothermal carbonization increased the thermal stability of the composites. This was to be expected since HTC resulted to the loss of some fractions of the substances which boil at 190°C during the 2hours HTC. Furthermore, the final percentage by weight of the residue varied with the polymer concentration.

3.3. Effect of Grinding Duration and % Absorbance of Sample

The effect of grinding duration and percentage of methylene blue adsorption for various sample compositions is shown on Table 4 and Figure 8. The results revealed that the duration of grinding has an effect on the percentage of methylene blue adsorption for various sample compositions. When the NMPs were coated with starch and pectin in the ratio 1:1, the maximum grinding time with best adsorption of 93.42 was 60 minutes, When peels replaced starch in the coating composition peels /pectin, the maximum grinding time with best adsorption of 97.46% was 30minutes While peels / starch, after 4 hours of grinding recorded a maximum, adsorption of 98.8%, When coated with peels alone, the maximum grinding time with best adsorption of 92.79% was 15minutes. These results indicated that modifying the synthesis conditions (i.e., the concentration of the aqueous saccharide solution (S: P ratio), the reaction time, and type of saccharide), modify the efficiency of the final adsorbent.

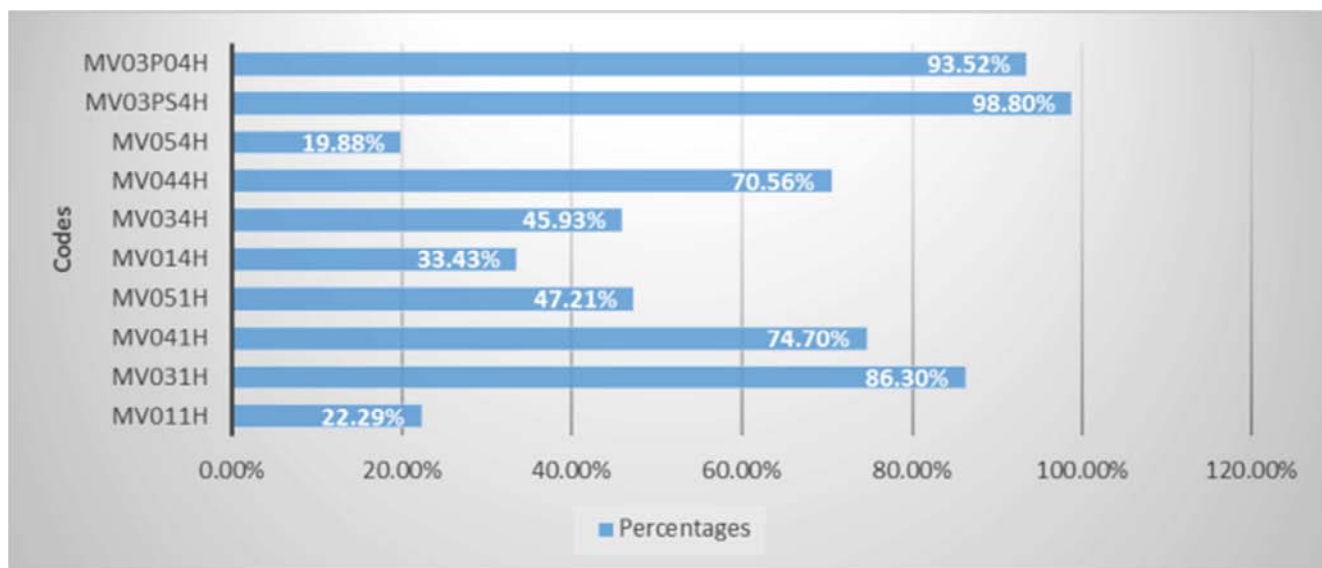


Figure 8. Effect of grinding time on sample % adsorbance.

Table 4. Oxide, polymer ratio MV01-MV05 and Clay, poly ratio MV07-MV10, composition of coating, grinding duration and % absorbance of sample.

Code	Description	Composition of coating substance	Mass	Grinding duration	Percentage absorbance
	Oxide: Polymer				
MV03PS	3:1	Peels used in place of pectin with starch	0.2g	15minutes	91.05
MV03PO	3:1	Peels used in place of pectin without starch		30minutes	81.22
MV03PO	3:1	Peels used for pectin without using starch		15minutes	92.79
MV03PS	3:1	Peels in place of pectin plus starch		30minutes	97.46
MV03	3:1	Pectin and starch used in the ratio 1:1	0.5g	1hr	93.42
MV03	3:1			4hours	54.75
MV05	Oxide only			15minutes	48.19
MV05	Oxide only			1hour	97.07
MV05	Oxide only			4hours	10.54
MV01	Polymer only			15minutes	46.53
MV01	Polymer only			1hour	36.05
MV01	Polymer only			4hours	67.35

3.4. The Influence of: Hydrothermal Carbonization, Polymer/Oxide, Pectin/Starch Ratio and Amount of Oxide on Methylene Blue Adsorption

The effects of hydrothermal carbonization are shown on Figures: 9 and 10. All the test samples in their pure forms showed adsorbance with respect to methylene blue dye. Pure clay (MV10) showed the highest percentage adsorbance of 96.57%, followed by the pure composite with adsorbance of 78%, the pure Iron Oxide (MV05B) with 48.19 % and polymer (MV01) with 43.3%. Hydrothermal carbonization at temperatures of 160-190°C for two hours has shown an effect on the absorbance of the test samples. The greatest increment was recorded on the polymer (MV01B, 46.7%) from 43.3 to 90%, followed by the pure Iron Oxide (MV05, 35.39%), from 48.19-83.5% while pure clay showed a decrease in the adsorbance (MV10B, -6.58%) from 96.57-89.99%. The

negative effect on pure clay is indicative of the fact that hydrothermal carbonization does not occur in the absence of the saccharides and the percentage increment in adsorbance may be proportional to the amount of char formed. This prediction was confirmed in MV07B and MV08B where with the presence of the polymer, (pectin and starch) an increment in the adsorbance was observed. This improvement was attributed to a carbon-rich solid product, here denoted as hydrochar which had been synthesized by the hydrothermal carbonization of two different saccharides (pectin and starch) at temperatures ranging from 160 to 190 °C. The microspheres thus obtained in the char possess, a highly aromatic nucleus (hydrophobic) and a hydrophilic shell containing a high concentration of reactive oxygen functional groups (i.e., hydroxyl/phenolic, carbonyl, or carboxylic which improve on the adsorbent capacity and efficiency of the original sample adsorbent).

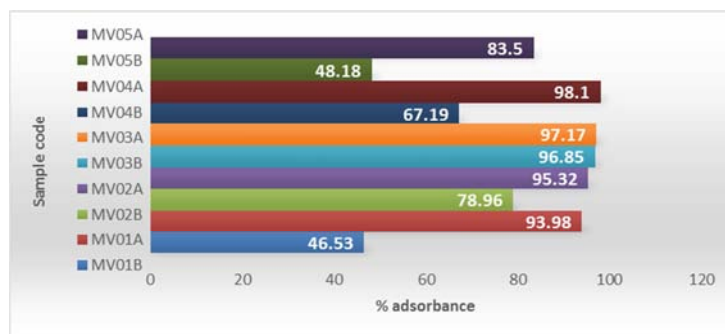


Figure 9. % absorbance before and after adsorption, for Iron Oxide based composites.



Figure 10. % absorbance before and after adsorption, for Clay based composites.

3.5. Influence of pH on Clay Composite (MV10) Adsorption of Methylene Blue

The influence of pH on dye removal was determined by performing the adsorption experiments at different initial pH of the solution (2-11) at room temperature. The pH of the solution was adjusted with HCl (0.1 N) or NaOH (0.1 N) solution by using a pH meter equipped with a combined pH electrode. The results as presented on Figure 11, indicated that the adsorption increased with increasing pH. The removal of the dye was low in the acid pH region which could be attributed to the fact that, hydrogen ions neutralize the negatively charged clay surface thereby decreasing the adsorption of the positively charged cations since there was reduction in the force of attraction between adsorbate and adsorbent. Conversely, removal of the dye was more at higher pH, because the surface of the used clay composite is negatively charged, therefore, the electrostatic attractive force between the colorant dye, which has a positive charge, and the adsorbent surface increased. Consequently, the rate of dye adsorption increased and the greatest dye removal was detected at pH 9. Similar results were reported in literature [22].

Concentration of MB=25mg/h, Adsorbent mass=0.5/

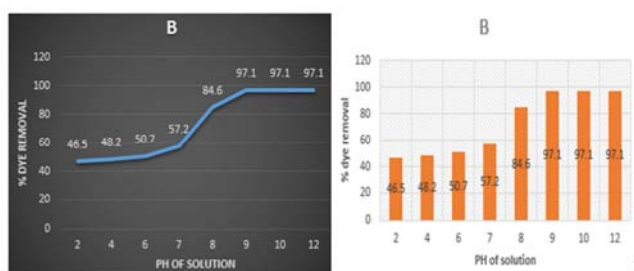


Figure 11. Showing the Influence of pH on % Methylene dye Adsorption (Clay composite).

3.6. Effect of Adsorbent Mass of Clay Composite (MV10) on Methylene Blue Adsorption

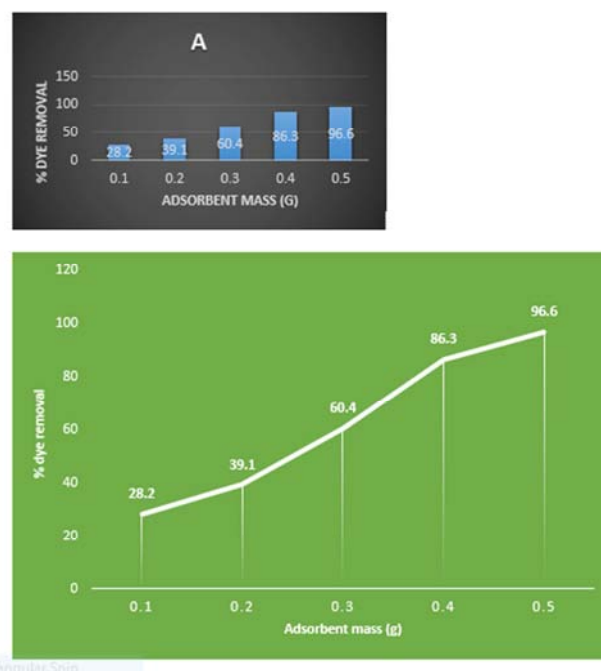


Figure 12. The effect of adsorbent mass of clay on the adsorption capacity.

The effect of adsorbent mass on the adsorption capacity was studied using 100 ml of Methylene blue (25mg/l) onto 0.1-0.5 g/l of adsorbent with shaking at room temperature for 30 min, the solid particles were removed and the remaining concentration of colorant in the filtrate was measured by using the UV/Vis spectrophotometer at 662 nm. The effect of sorbent quantity on dye removal is illustrated on Figure 12. It

was observed that increase in the mass of crude clay caused a decreases in residual dye concentration in the sampled dye polluted waste water for adsorbent masses in the range 0.1 g/l to 0.5 g/l. The increase in Methylene blue adsorption with the increase in adsorbent mass was attributed to increase in surface area of micro pores and the increase in availability of vacant adsorption sites. This observation agrees with those reported in literature [22].

Effect of adsorbent mass on methylene blue adsorption.

Concentration of MB=25mg/l, pH of solution=9

3.7. Effect of Contact Time on the Adsorbent

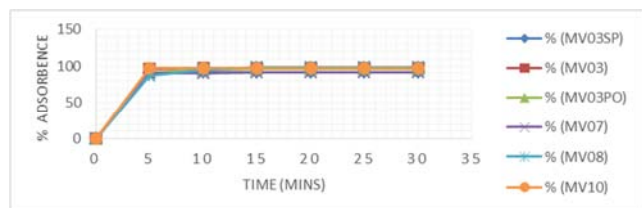


Figure 13. Effect of contact time on methyl blue adsorption onto Metal Oxide composite.

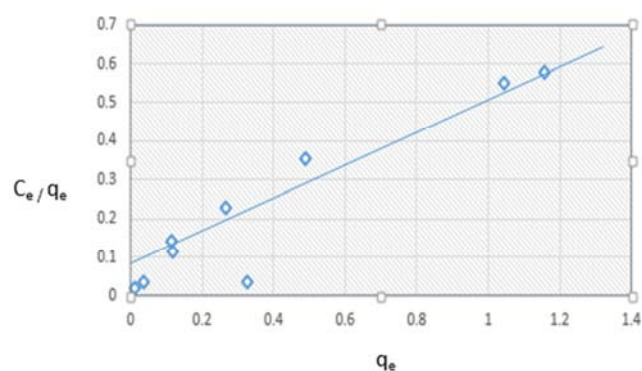


Figure 14. Langmuir isotherm showing Methyl blue removal at various equilibrium concentrations.

The effect of contact time on the adsorbent and Methylene blue is shown in Figures 13 and 14. The influence of contact time is a pertinent factor because it provides the relationship between fixed amounts of sorbent and contact time. It is used to estimate the sorption-desorption equilibrium contact time. The effect of time variation on the sorption capacity of samples for the removal of methylene blue (MB) has been investigated in the range of 0–100 min. A rapid increase in the sorption capacity of all the samples was noted during the first 10 min, and afterward, a very slow increase in the MB uptake was observed up to 30 min for all the samples. The maximum sorption capacity (97.89% Organo Iron Oxide composites and 98.8% for Organoclay composites) were determined at equilibrium time (30 min). The higher rates of sorption capacity of both Iron oxide based and clay based composites at the beginning could be attributed to the presence of a large number of sorption sites on the surface of the samples while low increase in sorption capacity was credited to the sorption sites which existed in the internal regions. At these points, the equilibrium times were attained. After the plateau, the surface pores of the adsorbent became

enclosed and desorption began such that the rate of adsorption was balanced by the rate of desorption. The slow rate of adsorption at this stage also known as the desorption process might have been due to the aggregation of methylene blue molecules on the surface of the adsorbent while enhanced sorption capacity of organoclay could be due to surfactant modification, which increased the carbon content of the sorbent.

Rates of Adsorption of Methylene Blue

The Langmuir adsorption isotherm shown on Figure 10b, assumes that monolayer adsorption exists at all surface sites which indicated homogeneity, with the ability of no interaction of adsorbed molecules with the neighbouring adsorption sites. The linear Langmuir equation is represented in equation (3):

$$\frac{ce}{qe} = \frac{1}{Qmb} + \frac{1}{Qm}C_e \quad (3)$$

Where C_e is the equilibrium concentration (mg/dm^3), q_e is the amount (mg/g) adsorbed at equilibrium time, and Q_m and b are Langmuir constants related to maximum adsorption capacity (mg/g) and energy of adsorption related to the heat of adsorption (L/mg), respectively. The Langmuir parameters were computed from the slopes and intercepts of the linear plot of C_e as the abscissa and C_e/q_e as the ordinate. The Langmuir isotherm parameters ($Q_m=2.360$ and $b=0.51674$) were used to calculate the affinity between the adsorbent and adsorbate via dimensionless separation factor, R_L , as determined using equation (4)

$$R_L = \frac{1}{1+bC_o} \quad (4)$$

Where b is the Langmuir constant and C_o is the initial concentration of metal ions. The R_L values promulgate whether the adsorption is irreversible ($R_L=0$), favorable ($0 < R_L < 1$) or linear / unfavorable ($R_L=1$ or $R_L > 1$). The values of R_L calculated for initial concentrations was 0.64202 which is an indication that the adsorption is favorable.

Adsorption kinetics

The adsorption kinetics and rate constants were determined from kinetic models including the pseudo-first-order and pseudo-second-order models. The pseudo-first-order and pseudo-second-order adsorption kinetics based on equilibrium adsorption are represented in equation (5)

$$\begin{aligned} \ln(q_e - q_t) &= \ln q_t - k_1 t \\ t / q_t &= (1/k_2 q_e^2) + (1/q_e) t \end{aligned} \quad (5)$$

Where q_e and q_t are the amounts of sample adsorbed onto the Composite (mg/g) at equilibrium and at a time, t , respectively. k_1 and k_2 are the rate constants for pseudo-first-order and pseudo-second-order kinetics, respectively. The first-order constant (min^{-1}) was determined in linear form by plotting $\ln(q_e - q_t)$ against t . A plot of q_t against t was used to determine pseudo-second-order constant (mg/g min).

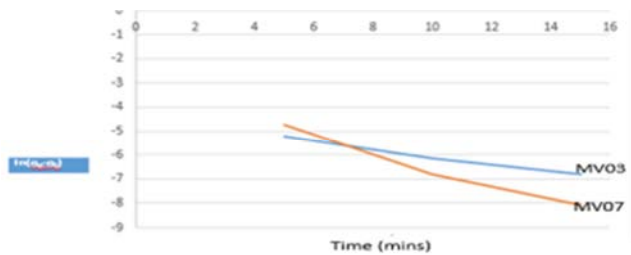


Figure 15. Pseudo-first-order plots for methylene blue removal at different times.

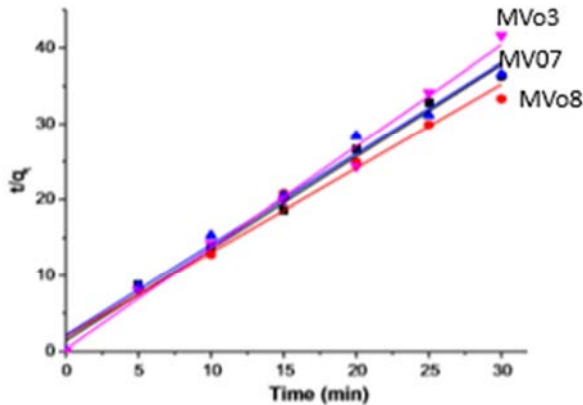


Figure 16. Pseudo-second-order plots for methylene blue removal at different times.

Adsorption kinetics provides information on the reaction pathways and the mechanisms of the adsorption of sorbate by the sorbent. The results obtained, described the kinetics of the adsorptions of studied samples (Iron Oxide composites) by using pseudo-first, Figure (15) and pseudo-second-order models Figure (16). For the pseudo-first-order model, the low k_1 values suggests that a slow adsorption process takes place, while for the pseudo-second order model, k_2 values were high indicating an increase in adsorption rates. The R_2 values for the adsorption kinetics of the methylene blue were higher for the pseudo-second-order model compared to those of the pseudo-first-order model. Thus, suggesting that, the pseudo-second-order model was a better model fitting the kinetics of the adsorption of the methylene blue employed in this study. Furthermore, in order to select a better model that fits the experimental data, Chi-square (χ^2), the mean square error (MSE), correlation coefficient (R^2) and the validation by the normalized standard deviation (q) listed in Table 5, were used to justify the favored adsorption kinetic model. The smaller the χ^2 value, the closer the agreement in the fit between the experimental data and linearized forms of the kinetic equations using the relationships in equation (6)

$$\begin{aligned}\chi^2 &= \sum_{i=1} (q_{e,exp} - q_{e,cal})^2 / q_{e,cal} \\ \text{MES} &= \frac{1}{n} \sum_{i=1} (q_{e,exp} - q_{e,cal})^2 \\ \Delta q (\%) &= \frac{100}{\sqrt{\frac{\sum_{i=1} (q_{e,exp} - q_{e,cal})^2}{N-1}}} \quad (6)\end{aligned}$$

Where N is the number of data points, $q_{e,exp}$ is the

experimental adsorption capacity and $q_{e,cal}$ is the calculated adsorption capacity. The results obtain here confirm that the pseudo second order model was the better model fitting the kinetics.

Table 5. Kinetic parameters of pseudo-first-order and pseudo second-order expressions.

Kinetic model	parameter	Sample code		
		MV03	MV07	MV08
pseudo-first-order model	χ^2	3.201	2.984	-
	MSE	2.1021	2.0032	-
	q	14.2201	13.9702	-
pseudo-second-order model	χ^2	0.03272	0.03391	0.3829
	MSE	0.00031	0.00039	0.00048
	q	3.6423	3.1849	3.2640

4. Conclusion

The preparation of a composite with a covalent biopolymer framework (CBF) was achieved by the formation of glycosidic linkages between pectin or peels and starch. Characterization of the covalent and ionic types of pectin–starch composites was supported by TGA results that revealed thermally stable cross-linked composites with a covalent frame work over the pectin–starch polyelectrolyte complex. The complex was converted to a hydrochar with hydrothermal carbonization which was even more stable due to the presence of the hydrophobic core and the hydrophilic shell. The IR intensity changes for the secondary carboxylate groups of starch before and after dye adsorption provided support to the fact that methylene blue was adsorbed by both the Iron Oxide/ Iron Oxide based composites from the magnetic sand as well as clay /clay based composites. The greater dye uptake capacity of pectin highlights the prominent role of the carboxylate anion site accessibility in the composites. The formation of a glycol-based covalent network results in greater pectin incorporation onto starch with secondary adsorption sites along the starch backbone. Pectin–starch composites as well as hydrothermal carbonization will contribute to the rational design of materials with improved properties for diverse adsorption-based applications. The adsorption properties of these samples can be modified using various composition ratios of functional materials such as peel, pectin/ starch, pH and Grinding/increase in grinding time to increase their affinity, selectivity, or degradation capacity towards targeted compounds. The adsorption kinetic of methylene blue onto MNPs can be better fitted by the linear Langmuir isotherm and the pseudo-second-order model was a better model fitting the kinetics of the adsorption of the methylene blue

Data Availability

All data used to support the findings of this study are included within the article.

Conflicts of Interest

There is no conflict of interest.

References

- [1] Kumar, K. V.; Ramamurthi, V.; Sivanesan, S. Modeling the mechanism involved during the sorption of methylene blue onto fly ash. *J. Colloid Interface Sci.* 2005, 284, 14–21. [CrossRef] [PubMed].
- [2] Low, K. S., C. K. Lee, and B. F. Tan, (2000). Quarternized wood as sorbent for reactive dyes. *Applied Biochemistry and Biotechnology*, 87, 233–245.
- [3] Tsai, W. T., H. C. Hsu, T. Y. Su, K. Y. Lin, and C. M. Lin, 2007. Removal of basic dye (methylene blue) from wastewaters utilizing beer brewery waste. *Journal of Hazardous Materials*, 154, 73–78.
- [4] Forgacs, E.; Cserh ti, T.; Oros, G. Removal of synthetic dyes from wastewaters: A review. *Environ. Int.* 2004, 30, 953–971. [CrossRef] [PubMed].
- [5] T n y, O.; Kabdasli, I.; Eremektar, G.; Orhon, D. Color removal from textile wastewaters. *Water Sci. Technol.* 1996, 34, 9–16.
- [6] Zhang, L.; Zeng, Y.; Cheng, Z. Removal of heavy metal ions using chitosan and modified chitosan: A review. *J. Mol. Liq.* 2016, 214, 175–191. [CrossRef]
- [7] Foba-Tendo J. Ngenefeme, Namanga J. Eko, Yufanyi D. Mbom, Ndinteh D. Tantoh, Krause W. M. Rui. A one pot green synthesis and characterization of Iron oxide-pectin hybrid nanocomposites, *Open Journal of Composite Materials*, 2013, 3, 30–37.
- [8] Chongrak Kaewprasit, Eric Hequet, Noureddine Abidi, and Jean Paul Gourmont. Application of methylene blue adsorption to cotton fibre specific surface Area measurement, *The Journal of Cotton Science* (1998) 2: 164–173.
- [9] M. Sundrarajan and M. Ramalakshmi. Novel cubic magnetite nanoparticles synthesis using room temperature Iron liquid, *E-Journal of Chemistry* 2012, 9 (3), 1070–1076.
- [10] Emmanuel Olajide Oyelude and Ursula Ruby Owusu. *Journal of applied science and environmental sanitation* (2011) Volume 6, Number 4: 477–484.
- [11] Auta, M.; Hameed, B. Modified mesoporous clay adsorbent for adsorption isotherm and kinetics of methylene blue. *Chem. Eng. J.* 2012, 198, 219–227, DOI: 10.1016/j.cej.2012.05.075.
- [12] Auta, M.; Hameed, B. Acid modified local clay beads as effective low-cost adsorbent for dynamic adsorption of methylene blue. *J. Ind. Eng. Chem.* 2013, 19, 1153–1161, DOI: 10.1016/j.jiec.2012.12.012.
- [13] Kismir, Y.; Aroguz, A. Z. Adsorption characteristics of the hazardous dye Brilliant Green on Saklıkent mud. *Chem. Eng. J.* 2011, 172, 199–206, DOI: 10.1016/j.cej.2011.05.090.
- [14] Nassar, M. M.; El-Geundi, M. S.; Al-Wahbi, A. A. Equilibrium modeling and thermodynamic parameters for adsorption of cationic dyes onto Yemen natural clay. *Desalin. Water Treat.* 2012, 44, 340–349, DOI: 10.1080/19443994.2012.691701.
- [15] Bai, T.; Zhao, K.; Gao, Q.; Qi, M.; Zhang, Y.; Lu, Z.; Zhao, H.; Gao, H.; Wei, J. Kaolin/CaAlg Hydrogel Thin Membrane with Controlled Thickness, High Mechanical Strength, and Good Repetitive Adsorption Performance for Dyes. *Ind. Eng. Chem. Res.* 2020, 59, 4958–4967, DOI: 10.1021/acs.iecr.9b06687 [ACS Full Text], [CAS], Google Scholar.
- [16] Yaqoob, S.; Ullah, F.; Mehmood, S.; Mahmood, T.; Ullah, M.; Khattak, A.; Zeb, M. A. Effect of waste water treated with TiO₂ nanoparticles on early seedling growth of Zea mays L. *J. Water Reuse Desalin.* 2018, 8, 424–431, DOI: 10.2166/wrd.2017.163 [Crossref], [CAS], Google Scholar.
- [17] Mih Venasius Nsom, Ekane Peter Etape, Josepha Foba Tendo, Beckley Victorine Namondo, Paul T. Chongwain, Mbom Divine Yufanyi, and Nzegge William. A Green and Facile Approach for Synthesis of Starch-Pectin Magnetite Nanoparticles and Application by Removal of Methylene Blue from Textile Effluent. *Journal of Nanomaterials*, Volume 2019, Article ID 4576135, 12 pages <https://doi.org/10.1155/2019/4576135>.
- [18] Li, M., Li, W. and Liu, S. X. (2011) Hydrothermal Synthesis, Characterization, and KOH Activation of Carbon Spheres from Glucose. *Carbohydrate Research*, 346, 999–1004. <http://dx.doi.org/10.1016/j.carres.2011.03.020>.
- [19] Kang, S., Li, X., Fan, J. and Chang, J. (2012) Characterization of Hydrochars Produced by Hydrothermal Carbonization of Lignin, Cellulose, d-Xylose, and Wood Meal. *Industrial and Engineering Chemistry Research*, 51, 9023–9031. <http://dx.doi.org/10.1021/ie300565d>.
- [20] Mosa, J., Dur n, A. and Aparicio, M. (2015) Sulfonic Acid-Functionalized Hybrid Organic-Inorganic Proton Exchange Membranes Synthesized by Sol-Gel Using 3-Mercaptopropyl Trimethoxysilane (MPTMS). *Journal of Power Sources*, 297, 208–216. <http://dx.doi.org/10.1016/j.jpowsour.2015.06.119>.
- [21] Xu, M. and Sheng, C. (2011) Influences of the Heat-Treatment Temperature and Inorganic Matter on Combustion Characteristics of Cornstalk Biochars. *Energy & Fuels*, 26, 209–218. <http://dx.doi.org/10.1021/ef2011657>.
- [22] Djelloul Bendaho, Tabet Ainad Driss and djillali Bassou (2015) Removal of Cationic Dye Methylene Blue from Aqueous Solution by Adsorption on Algerian Clay. *Int J Waste Resources* 2015, 5: 1 DOI: 10.4303/2252-5211.1000175.